Nanostructural Characterization of Large-Scale Porous Alumina Fabricated via Anodizing in Arsenic Acid Solution

Shunta Akiya, Tatsuya Kikuchi*, Shungo Natsui, and Ryosuke O. Suzuki
Faculty of Engineering, Hokkaido University
N13-W8, Kita-ku, Sapporo, Hokkaido, 060-8628, Japan

*Corresponding author: Tatsuya Kikuchi
TEL: +81-11-706-6340
FAX: +81-11-706-6342
E-mail: kiku@eng.hokudai.ac.jp

Abstract

Anodizing of aluminum in an arsenic acid solution is reported for the fabrication of anodic porous alumina. The highest potential difference (voltage) without oxide burning increased as the temperature and the concentration of the arsenic acid solution decreased, and a high anodizing potential difference of 340 V was achieved. An ordered porous alumina with several tens of cells was formed in 0.1-0.5 M arsenic acid solutions at 310-340 V for 20 h. However, the regularity of the porous alumina was not improved via anodizing for 72 h. No pore sealing behavior of the porous alumina was observed upon immersion in boiling distilled water, and it may be due to the formation of an insoluble complex on the oxide surface. The porous alumina consisted of two different layers: a hexagonal alumina layer that contained arsenic from the electrolyte and a pure alumina honeycomb skeleton. The porous alumina exhibited a white photoluminescence emission at approximately 515 nm under UV irradiation at 254 nm.

Keywords: Aluminum; Anodizing; Arsenic Acid; Porous Alumina; Nanostructure

1. Introduction

Anodizing (anodization) is the most important technique for surface finishing of aluminum and its alloys in various industrial applications, such as buildings [1], vehicles [2], and electronic devices [3]. Anodizing of aluminum in several acidic solutions under the appropriate operating conditions causes growth of the porous alumina (porous anodic oxide film) on the aluminum surface [4-9]. Porous alumina has a characteristic honeycomb nanostructure that consists of a porous layer with numerous high-aspect-ratio nanopores and a thin barrier layer. Therefore, porous alumina is widely used in various novel nano-science and engineering, such as storage devices [10], optoelectronic devices [11], metamaterials [12], photonic materials [13], surface plasmon resonances [14], gas sensors [15], biomaterials [16], and nanowires [17].

The chemical and physical properties and the nanomorphology of porous alumina strongly depend on the type of electrolyte species used during anodizing. For example, porous alumina formed in a sulfuric acid (H_2SO_4) solution possesses a relatively small cell size (interpore distance) measuring several tens of nanometers [18-20] and shows a high corrosion resistance after the pore sealing procedure of the porous layer [21]. Phosphoric acid (H_3PO_4) [22,23], chromic acid (H_2CrO_4) [24,25], oxalic acid (HOOC-COOH) [26,27], and other dicarboxylic acids [28-30] are widely recognized as suitable electrolytes for the formation of porous alumina.

Because the chemical and physical properties and the nanomorphology of porous alumina are still limited by a few typical electrolyte used during anodizing, the discovery of additional electrolytes would expand the applicability of porous alumina. For example, anodizing in etidronic and phosphonoacetic acid solutions can occur at high potential differences (voltage), i.e., >200 V [31-34], and produces a large-scale ordered porous alumina and generates a bright structural coloration from the nanostructured surface. Anodizing in pyrophosphoric acid ($H_4P_2O_7$) causes growth of single nanometer-scale alumina nanofibers, and the nanofiber-covered aluminum surface exhibits rapid superhydrophilicity [35-38]. Further additional electrolytes for anodizing allow the fabrication of novel anodic aluminum oxides with characteristic properties.

Selenic acid (H_2SeO_4) is a unique, new anodizing electrolyte for porous alumina [39-41]. Selenium is located below sulfur on the periodic table, and selenic acid is a strong diacid similar to sulfuric acid. The potential difference during anodizing with selenic acid is approximately twice as large as anodizing with sulfuric acid, and the resulting cell size of the porous alumina increased. On the basis of the sulfuric acid-selenic acid system and the experimental results obtained from anodizing with selenic acid, we focused on a new acidic electrolyte, arsenic acid (H_3AsO_4). Arsenic is located below phosphorus on the periodic table, and arsenic acid is a triprotic acid similar to phosphoric acid:

$$H_3AsO_4 \rightleftarrows H^+ + H_2AsO_4^- \quad (pKa_1 = 2.24) \quad (1)$$

$$H_2AsO_4^- \rightleftarrows H^+ + HAsO_4^{2-} \quad (pKa_2 = 6.94) \quad (2)$$

$$HAsO_4^{2-} \rightleftarrows H^+ + AsO_4^{3-} \quad (pKa_3 = 11.50) \quad (3)$$

where $pKa_{1, 2, 3}$ are the acid dissociation constants at 298 K [42]. Although these pKa values are slightly higher than those of phosphoric acid (pKa_1 = 1.83, pKa_2 = 6.43, pKa_3 = 11.46 at 298 K), arsenic acid may have potential as a suitable anodizing electrolyte for the formation of porous alumina because of its similar acid dissociation constants. In addition, higher potential difference anodizing may be achieved via anodizing with arsenic acid. The aim of this investigation is a) to demonstrate the growth behavior and nanostructural characterization of porous alumina formed via anodizing in a new electrolyte: arsenic acid solution, and b) to find novel characteristic properties of the porous alumina. This paper describes in detail the anodizing behavior of porous alumina during arsenic acid anodizing at extremely high potential differences. Simultaneously, we report a novel white photoluminescence emission from the porous alumina under ultraviolet irradiation.

2. Experimental

2.1 Pre-treatment of the aluminum specimens

Pure aluminum plates (99.999 wt%, 0.25-0.50 mm thick, GoodFellow, UK) were used as the anodizing specimens. The aluminum plates were cut into 5 mm × 20 mm pieces with a handle and were ultrasonically degreased in ethanol for 10 min at room temperature. After ultrasonication, the lower half of the handle was covered with a silicone resin (KE45W, Shin-Etsu, Japan) to prevent electrochemical reactions on the handle. The resin-coated specimens were electropolished in a 13.6 M CH_3COOH/2.56 M $HClO_4$ (78 vol% CH_3COOH/22 vol% 70%-$HClO_4$) solution at 280 K and 28 V for 1 min.

2.2 Arsenic acid anodizing

The electropolished aluminum specimens were used as the anode, and a platinum plate (26 mm × 25 mm, 99.95 wt%, Furuya Metal, Japan) was used as the cathode. The electrodes were immersed in 0.1-1.0 M arsenic acid solutions (150 mL, Kanto Chemical, Japan) at 273-293 K. The anode and cathode were 20 mm apart and parallel to each other in an electrochemical cell with an inner diameter measuring 55 mm. The arsenic solution was vigorously stirred at v = 814 rpm using a cross-head magnetic stir bar. The aluminum specimens were anodized at a constant current density of 1-50 Am^{-2} or at a constant potential difference (voltage) of 160-350 V for up to 72 h. A direct power supply (PWR400H, Kikusui Electronics, Japan) was used for each anodizing process, and the current density and potential difference were measured using the power supply and a digital multimeter (DMM4040, Tektronix, USA) connected to a PC. In the initial stage of constant potential difference anodizing, the potential difference was linearly increased for the first 2.5 min to avoid oxide burning as much as possible, and then maintained at each constant potential difference. After anodizing, the specimens were removed from the arsenic acid solution and were washed with distilled water. To compare the nanomorphologies of the porous alumina, we also anodized aluminum specimens in 0.3 M phosphoric acid at 273 K and in 0.3 M oxalic acid at 293 K.

2.3 Post-treatment of anodized specimens

After anodizing, several anodized specimens were boiled in distilled water at 373 K for 15 min to seal the nanopores in the porous alumina. The non-sealed specimens were immersed in a 0.2 M CrO_3/0.51 M H_3PO_4 solution at 353 K to dissolve the anodic oxide completely. The exposed aluminum substrate possessed a nanoscale dimple array configuration, which corresponded to the negative shape of the bottom of the porous alumina. The ordering behavior of the porous alumina was evaluated using fast Fourier transform (FFT) with the Image-J software package (Wayne Rasband, National Institute of Health, USA) [43-45]. After oxide dissolution, several nanostructured specimens were anodized again in arsenic acid solutions under the same operating conditions (two-step anodizing).

2.4 Characterization of the porous alumina

The anodized specimens were examined by field-emission scanning electron microscopy (FE-SEM, JSM-6500F, JEOL, Japan). To observe the porous alumina using SEM, we coated a thin platinum electroconductive layer onto the anodic oxide using a platinum sputter coater (MSP-1S, Vacuum Device, Japan). The anodized specimens were also examined by image-aberration-corrected scanning transmission electron microscopy (STEM, Titan G2 60-300, 300 kV, FEI). For the STEM observation of porous alumina, the specimens were prepared as follows (a–d): a) The porous alumina on one side of the specimen was covered with a corrosion-resistant sheet, and the specimen was immersed in a 2.5 M NaOH solution at room temperature. The porous alumina on the other side was completely dissolved, and the aluminum substrate was exposed to the solution. b) The aluminum-exposed specimens were immersed in a 0.5 M $SnCl_4$ solution at room temperature to completely dissolve the aluminum substrate. A free-standing porous alumina film was formed via these chemical dissolution processes. c) The porous alumina was fixed on a molybdenum single-hole grid (Nisshin EM, Japan) with an epoxy resin. d) The porous alumina was thinned via an argon-ion beam using a precision ion polishing system (PIPS, 5 kV, Gatan). The elemental distribution of aluminum, oxygen, arsenic, and phosphorus in the porous alumina was analyzed using energy-dispersive X-ray spectrometry (EDS).

The photoluminescence properties of the porous alumina were also examined using an ultraviolet (UV) mercury lamp (SLUV-8, 365 nm/254 nm, AS ONE, Japan) and a PC-controlled multi-channel spectrometer (USB2000+, Ocean Optics, USA). Three-dimensional photoluminescence maps were obtained by a fluorescence spectrometer (FP-8300, JASCO) with a 150 W xenon lamp as the excitation source (excitation range: 250-700 nm, emission range: 250-700 nm).

3. Results and Discussion

3.1 Constant current (CA) anodizing in arsenic acid solutions

Figure 1a shows the changes in the potential difference, U, with the anodizing time, t, during anodizing in a 0.5 M arsenic acid solution at 273 K and different current densities of 1-50 Am^{-2} for up to 20 h. At j = 1 Am^{-2}, the potential difference linearly increased to 210 V during the initial 5 h and then reached a steady value of 150 V after a slight decrease. The shape of the potential difference-time curve from CA anodizing can typically be measured via the growth of the porous alumina on the aluminum substrate [5,6]. When the current density increased to j = 2 Am^{-2}, the rate

of increase of the potential difference was approximately 2 times greater than that for j = 1 Am^{-2}. In addition, the potential difference reached a peak value of 310 V, and the overall value after the peak was approximately 100 V higher than that for j = 1 Am^{-2}. At larger current densities of j = 10 and 50 Am^{-2}, the potential differences reached 300 V or higher during anodizing. However, the potential differences for the initial stage when j = 10 Am^{-2} and for the whole stage at 50 Am^{-2} exhibited unstable oscillations. Several burning oxide spots with a black hue were formed on the aluminum specimen under these conditions.

Figure 1b shows an SEM image of the fracture cross-section of the specimen anodized in the 0.5 M arsenic acid solution at 273 K and 1 Am^{-2} for 20 h. The lower white area corresponds to the aluminum substrate; the middle stripe region corresponds to the anodic oxide; and the top gray surface corresponds to the surface of the anodic oxide. A porous alumina film with branching nanopores measuring 2.5 μm thick was uniformly formed on the aluminum substrate. Arsenic acid can easily create a porous alumina via CA anodizing, similar to phosphoric acid anodizing. Importantly, the potential difference during CA anodizing was greater than 300 V. Therefore, we examined constant potential difference anodizing in various arsenic acid solutions to identify the growth behavior of the large-scale porous alumina.

3.2 Constant potential difference (CPD) anodizing in arsenic acid solutions

Figure 2a shows the changes in the current density, j, with the anodizing time, t, at constant potential differences of 255-265 V in a 0.5 M arsenic acid solution at 293 K. In the CPD anodizing, the potential difference increased linearly during the first 2.5 min and was then held constant at each operating value to avoid oxide burning as much as possible. Therefore, a transient current density of approximately 50 Am^{-2} was measured during the first 2.5 min. After this transition period, the current densities decreased rapidly to approximately 5 Am^{-2}. The current decrease and stagnation are typically measured in the first stage during CPD anodizing. As the anodizing time increased to 15 min, the current densities increased rapidly and reached nearly steady values of approximately 70 Am^{-2} at 255 V and 85 Am^{-2} at 260 V. A uniform oxide film with a gray hue was formed on the aluminum specimen after anodizing at these potential differences. In contrast, the current density increased to greater than 200 Am^{-2} after 15-min-anodizing at 265 V, and a non-uniform oxide film with several black spots was formed on the surface via oxide burning.

Figure 2b and 2c show the current-time curves during anodizing in a 0.5 M arsenic acid solution at 283 K and 273 K, respectively. The length of the current stagnation in the initial stage of anodizing increased as the temperature decreased (15 min at 293 K, 30 min at 283 K, and 70 min at 273 K). In addition, the highest potential difference without oxide burning increased as the temperature decreased (260 V at 293 K, 285 V at 283 K, and 310 V at 273 K). These changes are due to the low solubility and the thickening of the barrier layer in the arsenic acid solutions at lower temperatures.

The authors and other research groups have reported previously that ordered porous alumina could be formed via anodizing at the highest potential difference without oxide burning [28,31]. Therefore, we used SEM to examine the regularity of the porous alumina formed via arsenic acid anodizing under the highest potential difference conditions. Figure 3 shows the exposed aluminum substrate after arsenic acid anodizing for 20 h at a) 260 V and 293 K, b) 285 V and 283 K, and c) 310 V and 273 K, as described in Fig. 2. Because the anodized specimens were immersed in a CrO_3/H_3PO_4 solution to completely dissolve the porous alumina, numerous aluminum dimples that corresponded to the bottom shape of the porous alumina were exposed to the surface in Fig. 3. At 260 V and 293 K (Fig. 3a), disordered aluminum dimples measuring approximately 200 nm to 1 μm in diameter were distributed over the surface, and the dimples exhibited various shapes, such as circles, pentagons, hexagons, and heptagons, on the array. The inset figure in the lower left of Fig. 3 shows the FFT image obtained from the aluminum dimple array. The FFT image exhibited a halo pattern based on the corresponding irregularity of the dimple array. As the anodizing temperature decreased to 283 K and 273 K and the highest potential difference increased to 285 V and 310 V (Figs. 3b and 3c), honeycomb dimple arrangements with several tens of hexagonal cells were observed on the surface. Although many defects still remained on the surface, the resulting FFT image with weak spots was observed because of the regularity of the porous alumina. At 310 V, the average dimple diameter was approximately 690 nm. The regularity of the porous alumina worsened with increasing temperature, which may have been due to irregular growth and pore branching in arsenic acid solutions at high temperatures. Phosphoric acid anodizing exhibits a similar tendency, and a low temperature phosphoric acid solution is generally used to form ordered porous alumina [22]. Therefore, the following investigations were performed in arsenic acid solutions at 273 K.

Figure 4 shows the current-time curves from the CPD anodizing in 0.1-1.0 M arsenic acid solutions at 273 K for up to 20 h. The highest potential difference decreased as the concentration of the arsenic acid solution increased (340 V in 0.1 M to 290 V in 1.0 M) because of thinning of the barrier layer during arsenic acid anodizing at high concentrations. In addition, the current density under the highest potential difference during anodizing increased with increasing concentration, and the growth rate of porous alumina is expected to increase as the concentration of the arsenic acid solution increases. The CPD methods demonstrated that arsenic acid anodizing allows for a high potential difference greater than 300 V. The corresponding aluminum dimple arrays formed under the highest potential difference conditions are shown at the bottom of Fig. 4. Disordered aluminum dimples with an FFT halo pattern were formed in a 1.0 M arsenic acid solution (Fig. 4d), similar to the results obtained via high temperature anodizing (Fig. 3a). This irregularity may also be due to pore branching during arsenic acid anodizing at high concentrations. In 0.1-0.5 M arsenic acid solutions (Figs. 4a-4c), slightly ordered dimple arrays with weak spots were observed on the surfaces. Large-scale dimples measuring approximately 740 nm in diameter were formed at 340 V. However, many defects remained on these dimple arrays. Figure 5 summarizes the changes in the highest potential difference with a) temperature and b) concentration during arsenic acid anodizing, and there are linear relationships.

During typical self-ordering anodizing using sulfuric, oxalic, phosphoric, selenic, or etidronic acid, ordered porous alumina can be fabricated via rearrangement of the cell configuration during long-term anodizing [46]. Figure 6a shows the current-time curve during CPD anodizing in a 0.3 M arsenic acid solution at 273 K and 320 V for up to 72 h; the corresponding dimple arrays formed after 1-72 h are shown in Figs. 6b-6e. The shape of the aluminum dimples after 1 h of anodizing was not clear (Fig. 6b) because no steady-state porous alumina growth was observed (Fig. 6a). A dimple array was clearly formed via 2.5 h of anodizing (Fig. 6c), and a honeycomb nanostructure with several tens of cells was formed via further anodizing for 10 h (Fig. 6d) and 72 h (Fig. 6e). However, the regularity of the dimple array was low after the 72 h anodizing, and a similar FFT pattern with weak spots was obtained. Highly ordered porous alumina with a wide-range honeycomb distribution could not be obtained via arsenic acid anodizing under any operating condition.

Why highly ordered porous alumina could not be fabricated via long-term arsenic acid anodizing is difficult to explain. In the high potential difference anodizing using citric acid and malic acid without imprint techniques, obtaining wide-region ordered porous alumina is hard. The same may be true in arsenic acid anodizing. In addition, the products formed via reduction on the cathode may be related to the disordering of porous alumina. During arsenic acid anodizing, gray arsenic deposits were formed on the platinum cathode due to the reduction of arsenate with hydrogen gas evolution. Electrodeposition on the cathode has also been observed in selenic acid anodizing (i.e., electrodeposition of selenium on the cathode) [39]. The adhesion of arsenic deposits to the cathode was inferior, and the arsenic deposits were easily removed from the cathode as small arsenic particles during anodizing. Figure 7 shows the appearance of the electrochemical cell after arsenic acid anodizing. The arsenic particles removed from the cathode were observed at the surface of the solution and on the stir bar. These arsenic particles also adhered to the aluminum specimen during the anodizing. Although the particles were easily washed away with distilled water after the anodizing, the adhesion of the arsenic particles may have negatively affected the growth and rearrangement of porous alumina. For fabrication of the ideal porous alumina, combine nanoimprinting techniques with short-time arsenic acid anodizing may be useful.

3.3 Pore sealing treatment of porous alumina

To protect aluminum and its alloys from corrosion, numerous nanopores in the porous alumina were sealed via immersion in boiling distilled water [47,48]. This process seals the nanopores through the hydration of the alumina and the subsequent volume expansion via the following chemical reaction:

$$Al_2O_3 + nH_2O \rightarrow Al_2O_3 \bullet nH_2O \qquad (4)$$

Figure 8 shows SEM images of the surface and fracture cross-section of the porous alumina before and after immersion in boiling distilled water for 15 min. To compare the pore sealing behaviors, we carried out a two-step anodizing in three different electrolyte solutions: a) oxalic acid (c = 0.3 M; U = 40 V; T = 293 K; first anodizing time, t_1 = 2 h; second anodizing time, t_2 = 10 min), b) phosphoric acid (0.3 M; 180 V; 273 K; 2 h; 10 min), and c) arsenic acid (0.3 M; 320 V; 273 K; 4 h; 4 h). Porous alumina measuring approximately 100 nm (oxalic acid), 450 nm (phosphoric acid), and 800 nm (arsenic acid) in cell diameter was formed on the aluminum specimens. When the specimen formed via oxalic acid anodizing was immersed in boiling distilled water for 15 min, numerous plate-like

boehmites measuring several hundreds of nanometers in width were formed on the surface of the porous alumina (pore sealing, Fig. 8a). Conversely, the nanostructural features of the porous alumina formed via phosphoric and arsenic acid anodizing remained unchanged after immersion in boiling water (Figs. 8b and 8c). The hydration rate of alumina formed via phosphoric acid anodizing was previously reported to be extremely slower than that formed via sulfuric and oxalic acid anodizing because of the formation of an insoluble complex on the oxide surface [49]. The reason why the porous alumina formed via arsenic acid anodizing could not be sealed may be related to the same considerations. However, pore sealing may be achieved via other sealing procedures using a nickel acetate or lithium hydroxide solution; further investigations are required.

3.4 Nanostructural characterization of the porous alumina

Figures 9a-9d show a HAADF-STEM image and the corresponding STEM-EDS elemental distribution maps (Al, O, and As) for the porous alumina formed via arsenic acid anodizing. The porous alumina was fabricated via a two-step anodizing in a 0.3 M arsenic acid solution at 273 K and 320 V for 20 h/4 h. From the HAADF-STEM image, the average diameter of the pores formed in the porous alumina was approximately 200 nm. Notably, the porous alumina consisted of white hexagonal oxides around the nanopores and a gray honeycomb skeleton. This contrast corresponded to the distribution of the arsenic in the porous alumina; i.e., the white hexagonal oxide contained arsenic, and the gray honeycomb skeleton consisted of almost pure alumina (Figs. 9b-9d). Figure 9e shows the aluminum, oxygen, and arsenic concentration profiles (at%) for the porous alumina; the amount of arsenic in the skeleton is clearly near zero. The arsenic content in the white hexagonal oxide is almost same, and the average arsenic atomic percent in the hexagonal oxide is approximately 9% (45%-AsO_4^{3-} and 55%-Al_2O_3). The TEM diffraction pattern indicates that the porous alumina consisted of an amorphous oxide (Fig. 9f).

The arsenic distribution is due to the incorporation of arsenate anions (AsO_4^{3-}) into the anodic oxide via a high electric field during arsenic acid anodizing. The incorporation depth of the anions into the oxide depends on the electrolyte species used during anodizing. For example, whereas sulfate anions (SO_4^{2-}) were incorporated into the cell boundary, phosphate anions (PO_4^{3-}) and etidronate anions ($C_2H_4O_7P_2^{4-}$) were incorporated into the middle of the oxide, and the honeycomb configuration without the anions was formed in the porous alumina [5,33]. Interestingly, the width of the skeleton formed via arsenic acid anodizing is much longer than that formed via other previously reported electrolyte species. The anion incorporation ratio, R_{ai}, into the porous alumina is defined as follows:

$$R_{ai} = 1 - (W_{sk} / D_{cell}) \qquad (5)$$

where W_{sk} corresponds to the width of the skeleton (the pure alumina region) and D_{cell} is the cell size (interpore distance) of the porous alumina. Specifically, the R_{ai} value increases as the anions are deeply incorporated into the oxide. The R_{ai} values for several electrolyte species decrease in the order [33,50,51]

Sulfate at 28 V (0.95) > Phosphate at 180 V (0.90) > Etidronate at 215 V (0.89) > Arsenate at 320 V (0.75)

The R_{ai} for the porous alumina formed via arsenic acid anodizing is small compared to the R_{ai} for the porous alumina formed via the other electrolytes. In addition, the R_{ai} value decreases with an increase in potential difference, and a relationship exists between the incorporation depth and the potential difference during anodizing.

Figure 10 shows the HAADF-STEM images and the corresponding elemental distribution maps of the porous alumina formed via anodizing in a) phosphoric acid and b) arsenic acid solutions. Here, the anodizing procedures were carried out under the same operating conditions (c = 0.3 M, T = 293 K, and U = 160 V), and a) phosphorus and b) arsenic were detected in the STEM-EDS analysis. In the phosphoric acid anodizing (Fig. 10a), phosphorus was deeply incorporated into the oxide and a thin alumina skeleton measuring 35-40 nm in width was formed in the matrix. In the arsenic acid anodizing (Fig. 10b), arsenic was distributed only at the nanopore surroundings and the pure alumina region was wider than that formed via phosphoric acid anodizing.

The difference in the depth of the incorporated anions depends on the electrolyte species used, because the same potential difference is applied to the aluminum specimen. The reason for this behavior is still unknown, and further investigations are required to elucidate the incorporation behavior of the anions into the porous alumina. However, we expect that the incorporation difficulty during arsenic acid anodizing is strongly related to the large size of arsenate anions compared to that of phosphate anions.

3.5 Photoluminescence properties of porous alumina

In this section, we describe our investigation of the photoluminescence emissions of the porous alumina formed via arsenic acid anodizing. Figure 11a shows the surface appearance of the porous alumina under white light and UV (365 nm and 254 nm wavelength) irradiation. The specimen was fabricated via the operating conditions described in Fig. 6 (c = 0.3 M, T = 273 K, U = 320 V, T = 72 h). The porous alumina exhibited a white hue under UV irradiation at 254 nm and no photoluminescence emission under UV irradiation at 365 nm. Figure 11b shows the photoluminescence spectra of the porous alumina under UV irradiation at 254 nm. For comparison, electropolished pure aluminum was also examined. On the electropolished aluminum surface without porous alumina, several peaks due to bright lines originating from the UV mercury lamp were measured. By contrast, an intense photoluminescence emission band with a center wavelength of approximately 515 nm was measured on the porous alumina.

It has been reported that several porous alumina films exhibit photoluminescence emission under UV irradiation [52-54]. Figure 12 shows excitation-emission-intensity maps of the porous alumina formed by anodizing in a) oxalic acid, b) phosphoric acid, and c) arsenic acid solutions. For the oxalic and phosphoric acid anodizing processes, the electropolished specimens were anodized in 0.3 M electrolyte solutions (293 K) at a constant current density of 20 Am^{-2} for 2 h. In the map for porous alumina formed by oxalic acid anodizing (Fig. 12a), a strong photoluminescence emission was identified at 300-450 nm range in excitation and 400-500 nm range in emission. Porous alumina films formed by organic carboxylic electrolytes such as oxalic and malonic acid exhibit such a blue photoluminescence emission [52, 55-58]. Although the reason of the photoluminescence emission from porous alumina is still controversial, it is considered that the emission is generated from a) F^+ centers (oxygen vacancies in aluminum oxide) and b) F centers (incorporated anion vacancies originating from the electrolyte during anodizing) [55-57]. In the case of phosphoric acid anodizing (Fig. 12b), an extremely weak peak was measured at approximately 370 nm in excitation and 430 nm in emission, and no visible photoluminescence emission was observed [55]. In contrast, a characteristic broad peak (250-280 nm range in excitation and 400-700 nm range in emission) was measured from the porous alumina formed by arsenic acid anodizing (Fig. 12c). The white hue from the porous alumina (Fig. 11a) corresponds to this broad photoluminescence emission with visible regions of 400-700 nm. The white photoluminescence emission may be due to the arsenate anion vacancies incorporated from the electrolyte solution during anodizing (Fig. 9). However, the difference between the effect of phosphate (PO_4^{3-}) and arsenate anions (AsO_4^{3-}) on the photoluminescence behavior is still unknown; thus, further investigations are required.

The use of arsenic acid may be limited to particular applications such as a closed system due to their toxicity. However, our new findings in this investigation will contribute to the discussion on the anodizing science/technology and photoluminescence emission. White-light emission under UV irradiation is very interesting for potential applications in various light-emitting devices.

4. Conclusions

We demonstrated the anodizing of aluminum in a new electrolyte, an arsenic acid solution. The following conclusions were drawn from the results of our investigation.

1) A porous alumina was formed on the aluminum surface via CA and CPD anodizing in arsenic acid solutions.
2) The highest potential difference without oxide burning increases as the temperature and concentration of the arsenic acid solution decrease. A CPD anodizing at 340 V can be conducted in a 0.1 M arsenic acid solution at 273 K.
3) An ordered cell configuration with several tens of cells was formed via anodizing in 0.1-0.5 M arsenic acid solutions at each of the highest potential differences for 20 h. However, the regularity of the porous alumina was nearly unchanged for the 72 h anodizing.
4) No pore sealing behavior of the porous alumina was observed upon immersion in boiling distilled water for 15 min.
5) The porous alumina consists of an alumina/arsenic composite layer that originates from the electrolyte solution and a pure alumina skeleton. The skeleton is much thicker than the skeletons formed via other typical anodizing procedures.
6) The porous alumina exhibits a white photoluminescence emission with a center wavelength of approximately 515 nm under UV irradiation at 254 nm.

Acknowledgments

This study was conducted at Hokkaido University and was supported by the “Nanotechnology

Platform" Program of the Ministry of Education, Culture, Sports, Science, and Technology (MEXT), Japan. The authors would like to thank Mr. Nobuyuki Miyazaki, Mr. Takashi Endo, and Mr. Ryo Oota for their assistance in the SEM and STEM observations. This study was financially supported by the Light Metal Educational Foundation, Japan, the Sumitomo Foundation, Japan, and the Japan Society for the Promotion of Science (JSPS) "KAKENHI".

References

1) S. Khairnasov, B. Rassamakin, R. Musiy, A. Rassamakin, Solar collectors of buildings facade based on aluminum heat pipes with colored coating, Journal of Civil Engineering and Architecture 7 (2013) 403-408.
2) T. Kikuchi, Y. Hara, M. Sakairi, T. Yonezawa, A. Yamauchi, H. Takahashi, Corrosion of Al–Sn–Bi alloys in alcohols at high temperatures. Part II: Effect of anodizing on corrosion, Corrosion Science, 52 (2011) 2525-2534.
3) Z. Ashitaka, G.E. Thompson, P. Skeldon, G.C. Wood, K. Shimizu, The Behavior of Copper and Lead during Heat-Treatment and Surface Treatment of Aluminium Capacitor Foils, Journal of The Electrochemical Society, 146 (1999) 1380-1385.
4) K. Watanabe, M. Sakairi, H. Takahashi, S. Hirai, S. Yamaguchi, Formation of Al–Zr composite oxide films on aluminum by sol–gel coating and anodizing, Journal of Electroanalytical Chemistry, 473 (1999) 250-255.
5) W. Lee, S.-J. Park, Porous anodic aluminum oxide: anodization and templated synthesis of functional nanostructures, Chemical Reviews 114 (2014) 7487-7556.
6) G.D. Sulka, Highly ordered anodic porous alumina formation by self-organized anodizing, in: A. Eftekhari (Ed.), Nanostructured Materials in Electrochemistry, Wiley-VCH, 2008, p. 1.
7) G.E. Thompson, Porous anodic alumina: fabrication, characterization and applications, Thin Solid Films 297 (1997) 192-201.
8) J.E. Houser, K.R. Hebert, The role of viscous flow of oxide in the growth of self-ordered porous anodic alumina films, Nature Materials 8 (2009) 415-420.
9) K.R. Hebert, S.P. Albu, I. Paramasivam, P. Schmuki, Morphological instability leading to formation of porous anodic oxide films, Nature Materials 11 (2012) 162-166.
10) W. Lee, H. Han, A. Lotnyk, M.A. Schubert, S. Senz, M. Alexe, D. Hesse, S. Baik, U. Gösele, Individually addressable epitaxial ferroelectric nanocapacitor arrays with near Tb inch^{-2} density, Nature Nanotechnology 3 (2008) 402-407.
11) T. Ozel, G.R. Bourret, C.A. Mirkin, Coaxial lithography, Nature Nanotechnology 10 (2015) 319-324.
12) J. Yao, Z. Liu, Y. Liu, Y. Wang, C. Sun, G. Bartal, A.M. Stacy, X. Zhang, Optical negative refraction in bulk metamaterials of nanowires, Science 321 (2008) 930.
13) J. Martín, M. Martín-González, J.F. Fernández, O. Caballero-Calero, Ordered three-dimensional interconnected nanoarchitectures in anodic porous alumina, Nature Communications 5 (2014) 5130.
14) T. Kondo, N. Kitagishi, T. Yanagishita, H. Masuda, Surface-enhanced Raman scattering on gold nanowire array formed by mechanical deformation using anodic porous alumina molds, Applied Physics Express 8 (2015) 062002.
15) A. Mozalev, M. Bendova, R.M. Vazquez, Z. Pytlicek, E. Llobet, J. Hubalek, Formation and gas-sensing properties of a porous-alumina-assisted 3-D niobium-oxide nanofilm, Sensors and Actuators B: Chemical 229 (2016) 587-598.
16) X. Zhao, G. Meng, F. Han, X. Li, B. Chen, Q. Xu, X. Zhu, Z, Chu, M. Kong, Q. Huang, Nanocontainers made of various materials with tunable shape and size, Scientific Reports 3 (2013) 2238.
17) T. Kondo, N. Kitagishi, T. Fukushima, T. Yanagishita, H. Masuda, Fabrication of aluminum nanowires by mechanical deformation of Al using anodic porous alumina molds, Materials Express 6 (2016) 363-366.
18) H. Masuda, F. Hasegawa, S. Ono, Self-Ordering of Cell Arrangement of Anodic Porous Alumina Formed in Sulfuric Acid Solution, Journal of The Electrochemical Society 144 (1997) L127-L310.
19) H. Asoh, K. Nishio, M. Nakao, A. Yokoo, T. Tamamura, H. Masuda, Fabrication of ideally ordered anodic porous alumina with 63 nm hole periodicity using sulfuric acid, Journal of Vacuum Science & Technology B 19 (2001) 569-572.
20) G.D. Sulka, S. Stroobants, V. Moshchalkov, G. Borghs, J.P. Celis, Synthesis of well-ordered nanopores by anodizing aluminum foils in sulfuric acid, Journal of The Electrochemical Society 149 (2002) D97-D103.
21) J.A. Gonzalez, V. Lopez, E. Otero, A. Bautista, Postsealing changes in porous aluminum oxide films obtained in sulfuric acid solutions, Journal of The Electrochemical Society 147 (2000) 984-990.
22) H. Masuda, K. Yada, A. Osaka, Self-ordering of cell configuration of anodic porous alumina with large-size pores in phosphoric acid solution, Japanese Journal of Applied Physics 37 (1998)

L1340.
23) L. Zaraska, G.D. Sulka, M. Jaskuła, The effect of n-alcohols on porous anodic alumina formed by self-organized two-step anodizing of aluminum in phosphoric acid, Surface and Coatings Technology 204 (2010) 1729-1737.
24) S.J. Garcia-Vergara, P. Skeldon, G.E. Thompson, H. Habazaki, A tracer investigation of chromic acid anodizing of aluminium, Surface and Interface Analysis 39 (2007) 860-864.
25) W.J. Stępniowski, M. Michalska-Domańska, M. Norek, T. Czujko, Fast Fourier transform based arrangement analysis of poorly organized alumina nanopores formed via self-organized anodization in chromic acid, Materials Letters 117 (2014) 69-73.
26) H. Asoh, K. Nishio, M. Nakao, T. Tamamura, H. Masuda, Conditions for fabrication of ideally ordered anodic porous alumina using pretextured Al, Journal of The Electrochemical Society 148 (2001) B152-B156.
27) A. Mozalev, A. Poznyak, I. Mozaleva, A.W. Hassel, The voltage–time behaviour for porous anodizing of aluminium in a fluoride-containing oxalic acid electrolyte, Electrochemistry communications 3 (2001) 299-305.
28) S. Ono, M. Saito, H. Asoh, Self-ordering of anodic porous alumina formed in organic acid electrolytes, Electrochimica Acta 51 (2005) 827-833.
29) S.Z. Chu, K. Wada, S. Inoue, M. Isogai, Y. Katsuta, A. Yasumori, Large-scale fabrication of ordered nanoporous alumina films with arbitrary pore intervals by critical-potential anodization, Journal of The Electrochemical Society 153 (2006) B384-B391.
30) M. Pashchanka, J.J. Schneider, Experimental validation of the novel theory explaining self-organization in porous anodic alumina films, Physical Chemistry Chemical Physics 15 (2013) 7070-7074.
31) T. Kikuchi, O. Nishinaga, S. Natsui, R.O. Suzuki, Fabrication of self-ordered porous alumina via etidronic acid anodizing and structural color generation from submicrometer-scale dimple array, Electrochimica Acta 156 (2015) 235-243.
32) T. Kikuchi, O. Nishinaga, S. Natsui, R.O. Suzuki, Polymer nanoimprinting using an anodized aluminum mold for structural coloration, Applied Surface Science 341 (2015) 19-27.
33) A. Takenaga, T. Kikuchi, S. Natsui, R.O. Suzuki, Exploration for the Self-ordering of Porous Alumina Fabricated via Anodizing in Etidronic Acid, Electrochimica Acta 211 (2016) 515-523.
34) A. Takenaga, T. Kikuchi, S. Natsui, R.O. Suzuki, Self-ordered aluminum anodizing in phosphonoacetic acid and its structural coloration, ECS Solid State Letters 4 (2015) P55-P58.
35) T. Kikuchi, O. Nishinaga, D. Nakajima, J. Kawashima, S. Natsui, N. Sakaguchi, R.O. Suzuki, Ultra-high density single nanometer-scale anodic alumina nanofibers fabricated by pyrophosphoric acid anodizing, Scientific reports, 4 (2014) 7411.
36) D. Nakajima, T. Kikuchi, S. Natsui, N. Sakaguchi, R.O. Suzuki, Fabrication of a novel aluminum surface covered by numerous high-aspect-ratio anodic alumina nanofibers, Applied Surface Science 356 (2015) 54-62.
37) D. Nakajima, T. Kikuchi, S. Natsui, R.O. Suzuki, Highly Ordered Anodic Alumina Nanofibers Fabricated via Two Distinct Anodizing Processes, ECS Electrochemistry Letters 4 (2015) H14-H17.
38) D. Nakajima, T. Kikuchi, S. Natsui, R.O. Suzuki, Superhydrophilicity of a nanofiber-covered aluminum surface fabricated via pyrophosphoric acid anodizing, Applied Surface Science 389 (2016) 173-180.
39) O. Nishinaga, T. Kikuchi, S. Natsui, R.O. Suzuki, Rapid fabrication of self-ordered porous alumina with 10-/sub-10-nm-scale nanostructures by selenic acid anodizing, Scientific reports 3 (2013) 2748.
40) T. Kikuchi, O. Nishinaga, S. Natsui, R.O. Suzuki, Self-ordering behavior of anodic porous alumina via selenic acid anodizing, Electrochimica Acta 137 (2014) 728-735.
41) S. Akiya, T. Kikuchi, S. Natsui, R.O. Suzuki, Optimum exploration for the self-ordering of anodic porous alumina formed via selenic acid anodizing, Journal of The Electrochemical Society 162 (2015) E244-E250.
42) Y. Iwasawa, Handbook of Chemistry, Pure chemistry-II, fifth ed., Maruzen, Tokyo, 2004. P. 333.
43) M. Norek, W.J. Stępniowski, D. Siemiaszko, Effect of ethylene glycol on morphology of anodic alumina prepared in hard anodization, Journal of Electroanalytical Chemistry 762 (2016) 20-28.
44) W.J. Stępniowski, A. Nowak-Stępniowska, A. Presz, T. Czujko, R.A. Varin, The effects of time and temperature on the arrangement of anodic aluminum oxide nanopores, Materials characterization 91 (2014) 1-9.

45) W.J. Stępniowski, M. Norek, M. Michalska-Domańska, D. Forbot, A. Król, Study on the correlation between criterion number derived from Rayleigh–Bénard convective cells and arrangement of nanoporous anodic aluminum oxide, Materials Letters 125 (2014) 124-127.
46) H. Masuda, K. Fukuda, Ordered metal nanohole arrays made by a two-step replication of honeycomb structures of anodic alumina, Science 268 (1995) 1466-1468.
47) V. Lopez, E. Otero, A. Bautista, J.A. Gonzalez, Sealing of anodic films obtained in oxalic acid baths, Surface and Coatings Technology 124 (2000) 76-84.
48) J.A. Gonzalez, V. Lopez, E. Otero, A. Bautista, Postsealing changes in porous aluminum oxide films obtained in sulfuric acid solutions, Journal of The Electrochemical Society 147 (2000) 984-990.
49) S. Ono, N. Masuko, The Effect of Incorporated Anions to the Sealing of Porous Anodic Films on Aluminum, Journal of the Surface Finishing Society of Japan 45 (1994) 1070-1071.
50) R. Kondo, T. Kikuchi, S. Natsui, R.O. Suzuki, Fabrication of self-ordered porous alumina via anodizing in sulfate solutions, Materials Letters 183 (2016) 285-289.
51) F. Le Coz, L. Arurault, L. Datas, Chemical analysis of a single basic cell of porous anodic aluminium oxide templates, Materials characterization 61 (2010) 283-288.
52) Y. Yamamoto, N. Baba, S. Tajima, Coloured materials and photoluminescence centres in anodic film on aluminium, Nature 289 (1981) 572-574.
53) I.K. Chin, F.K. Yam, Y. Chai, Z. Hassan, Quantitative analysis of morphological and photoluminescence properties of porous anodic alumina formed in sulfuric acid, Journal of Porous Materials, 22 (2015) 1375-1382.
54) W.J. Stępniowski, M. Norek, M. Michalska-Domańska, A. Nowak-Stępniowska, M. Kaliszewski, A. Bombalska, Z. Bojar, Fabrication and Luminescence of Anodic Alumina with Incorporated Vanadyl Citrate Chelate Anions, Journal of Materials Science and Nanotechnology 1 (2014) 1.
55) Z. Li, K. Huang, Blue luminescence in porous anodic alumina films, Journal of Physics: Condensed Matter 19 (2007) 216203.
56) A. Santos, M. Alba, M.M. Rahman, P. Formentín, J. Ferré-Borrull, J. Pallarès, L.F. Marsal, Structural tuning of photoluminescence in nanoporous anodic alumina by hard anodization in oxalic and malonic acids, Nanoscale research letters 7 (2012) 228.
57) G.S. Huang, X.L. Wu, Y.F. Mei, X.F. Shao, G.G. Siu, Strong blue emission from anodic alumina membranes with ordered nanopore array, Journal of applied physics 93 (2003) 582-585.
58) S. Tajima, N. Baba, K. Shimizu, I. Mizuki, Photoluminescence of anodic oxide films on aluminium, Active and Passive Electronic Components 3 (1976) 91-95.

Figures

Fig. 1 a) Changes in the potential difference, U, with time, t, during aluminum anodizing in a 0.5 M arsenic acid solution at 273 K and different current densities from 1-50 Am^{-2}. b) An SEM image of the fracture cross-section of the porous alumina formed at 1 Am^{-2} after 20 h.

Fig. 2 Changes in the current density, j, with time, t, during CPD anodizing in a 0.5 M arsenic acid solution at a) 293 K, b) 283 K, and c) 273 K.

Fig. 3 SEM images of the nanostructured aluminum surface after arsenic acid anodizing and subsequent oxide dissolution. The inset figures show the resulting FFT image obtained from the aluminum dimple array.

Fig. 4 Changes in the current density, j, with time, t, during CPD anodizing in a) 0.1, b) 0.3, c) 0.5, and d) 1.0 M arsenic acid solutions at 293 K. The bottom SEM images show the nanostructured aluminum surface formed via each highest potential difference anodizing for 20 h.

Fig. 5 Changes in the highest potential difference with a) temperature and b) concentration during arsenic acid anodizing.

Fig. 6 a) Changes in the current density, j, with time, t, during CPD anodizing in a 0.3 M arsenic acid solution at 273 K and 320 V. b)-e) SEM images of the aluminum dimple array formed via arsenic acid anodizing for b) 1 h, c) 2.5 h, d) 10 h, and e) 72 h.

Fig. 7 Appearance of the electrochemical cell after the arsenic acid anodizing.

Fig. 8 SEM images of the surface and fracture cross-section of the porous alumina before/after immersion in boiled distilled water for 15 min. To compare the pore sealing behaviors, anodizing was carried out in a) oxalic acid, b) phosphoric acid, and c) arsenic acid solutions.

Fig. 9 a) A HAADF-STEM image, b)-d) the corresponding STEM-EDS elemental maps of aluminum, oxygen, and arsenic, e) EDS line profiles for each element, and f) a diffraction pattern of the porous alumina fabricated via two-step anodizing in a 0.3 M arsenic acid solution at 273 K and 320 V for 20 h/4 h.

Fig. 10 HAADF-STEM images and the corresponding STEM-EDS elemental maps for the porous alumina fabricated via a) phosphoric acid and b) arsenic acid anodizing. The anodizing conditions were c = 0.3 M, T = 293 K, and U = 160 V.

Fig. 11 a) Surface appearance of the porous alumina formed via arsenic acid anodizing under white-light and UV (365 nm and 254 nm) irradiation. b) The photoluminescence spectra of the porous alumina under UV irradiation at 254 nm. The reflection spectrum from the electropolished aluminum is also shown.

Fig. 12 Excitation-emission-intensity maps of the porous alumina formed by anodizing in a) oxalic acid, b) phosphoric acid, and c) arsenic acid solutions. The scale to the right indicates the relative intensity of the photoluminescence emission.

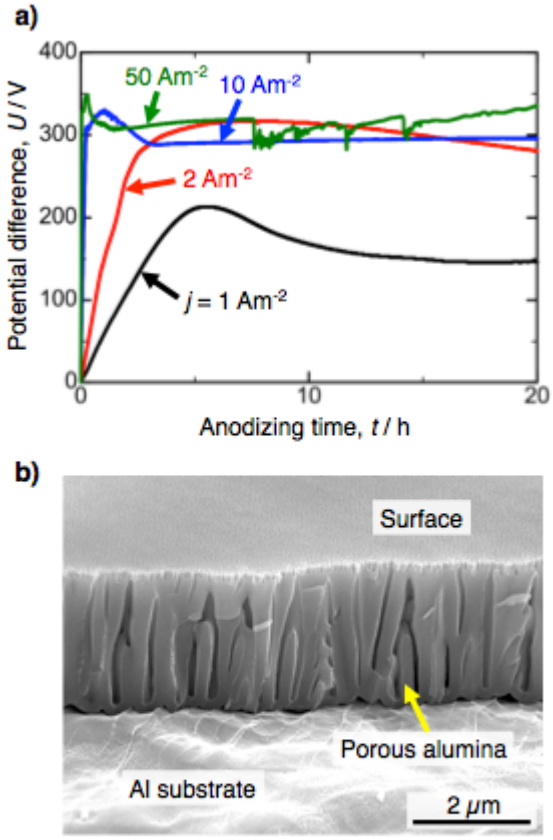
a)
400
300
200
100
0
Potential difference, U / V
50 Am-2
10 Am-2
2 Am-2
j = 1 Am-2
0
10
20
Anodizing time, t / h
b)
Surface
Porous alumina
Al substrate
2 μm

Figure 1.

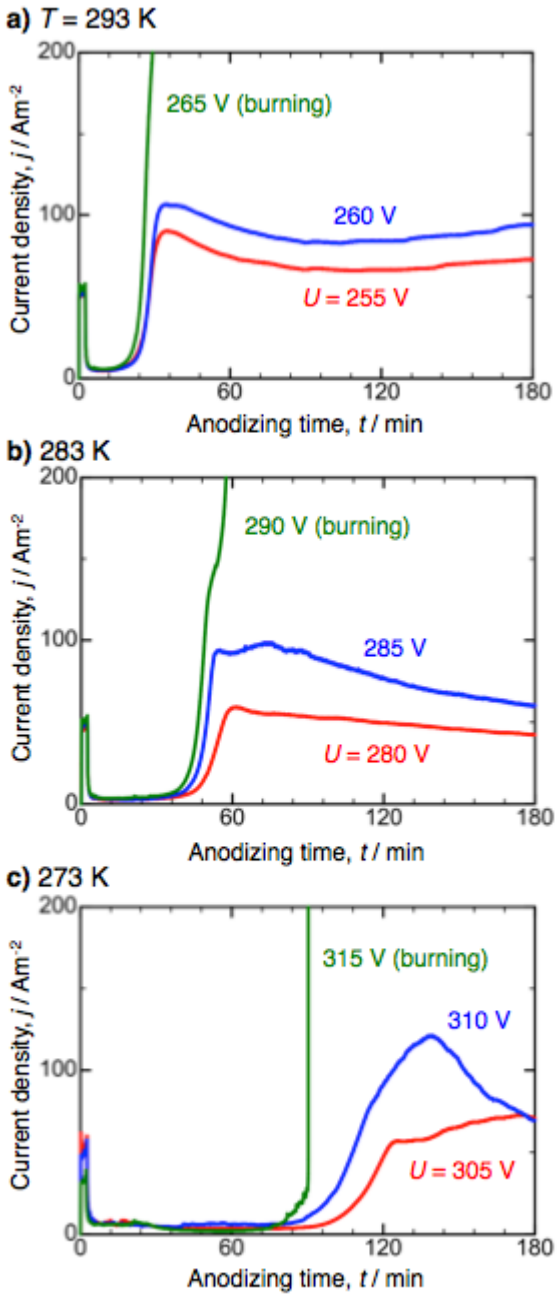
a) T = 293 K
265 V (burning)
260 V
U = 255 V
Current density, j / Am-2
Anodizing time, t / min
b) 283 K
290 V (burning)
285 V
U = 280 V
Current density, j / Am-2
Anodizing time, t / min
c) 273 K
315 V (burning)
310 V
U = 305 V
Current density, j / Am-2
Anodizing time, t / min

Figure 2.

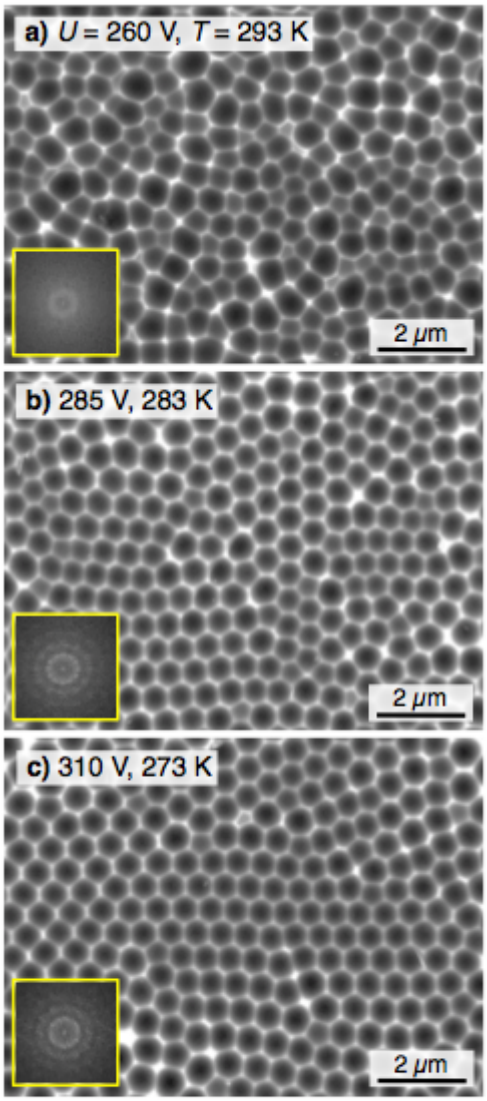

Figure 3.

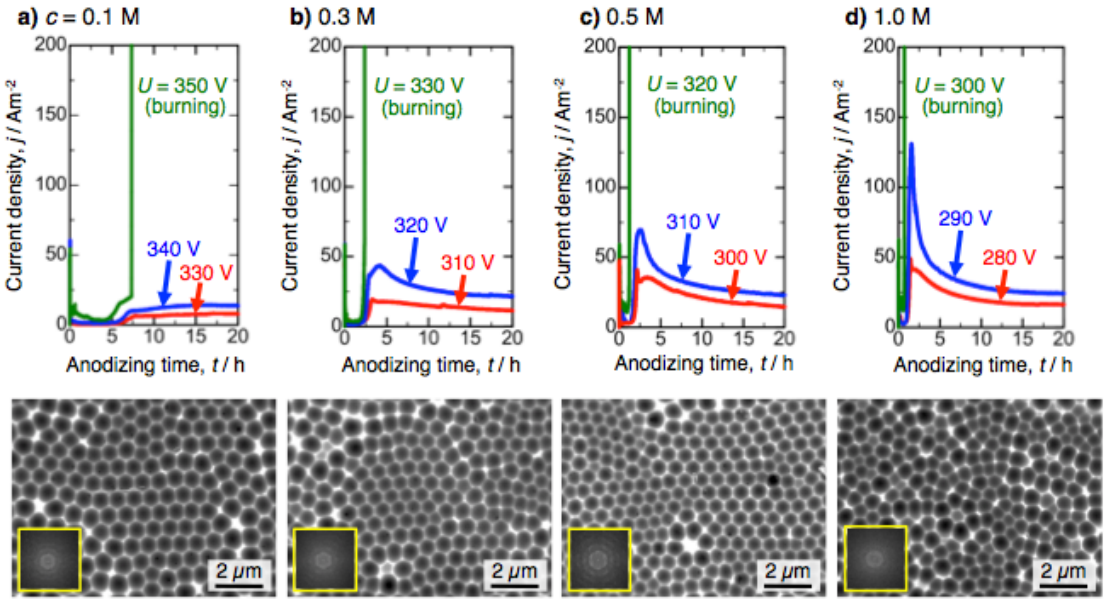
a) c = 0.1 M
b) 0.3 M
c) 0.5 M
d) 1.0 M
Current density, j / Am-2
Anodizing time, t / h
U = 350 V (burning)
340 V
330 V
U = 330 V (burning)
320 V
310 V
U = 320 V (burning)
310 V
300 V
U = 300 V (burning)
290 V
280 V
2 µm

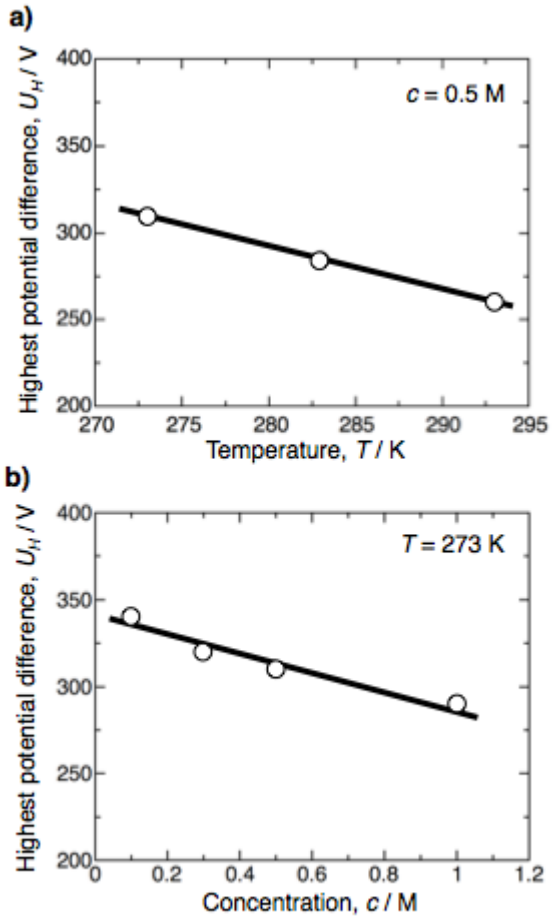
a)
Highest potential difference, U_H / V
400
350
300
250
200
c = 0.5 M
270
275
280
285
290
295
Temperature, T / K
b)
Highest potential difference, U_H / V
400
350
300
250
200
T = 273 K
0
0.2
0.4
0.6
0.8
1
1.2
Concentration, c / M

Figure 5.

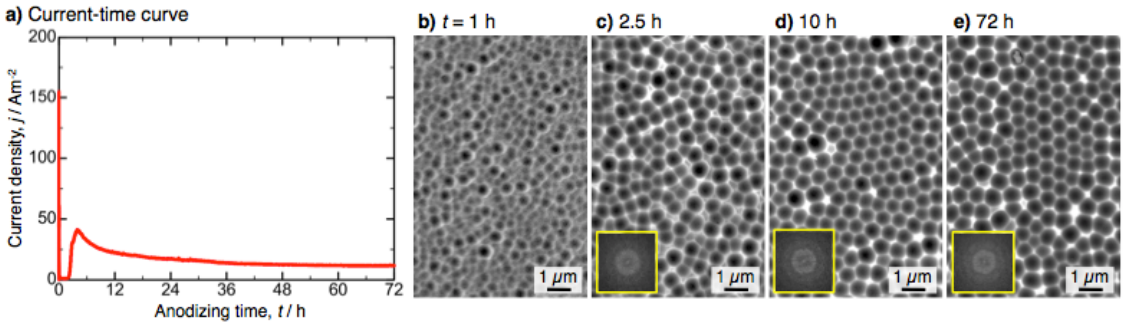
a) Current-time curve
Current density, j / Am-2
200
150
100
50
0
0
12
24
36
48
60
72
Anodizing time, t / h
b) t = 1 h
c) 2.5 h
d) 10 h
e) 72 h
1 µm
1 µm
1 µm
1 µm

Figure 6.

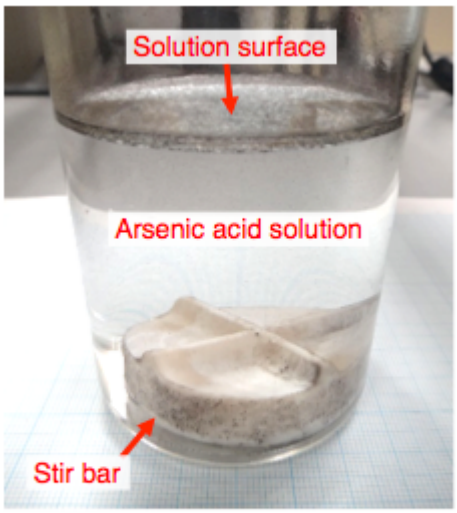

Figure 7.

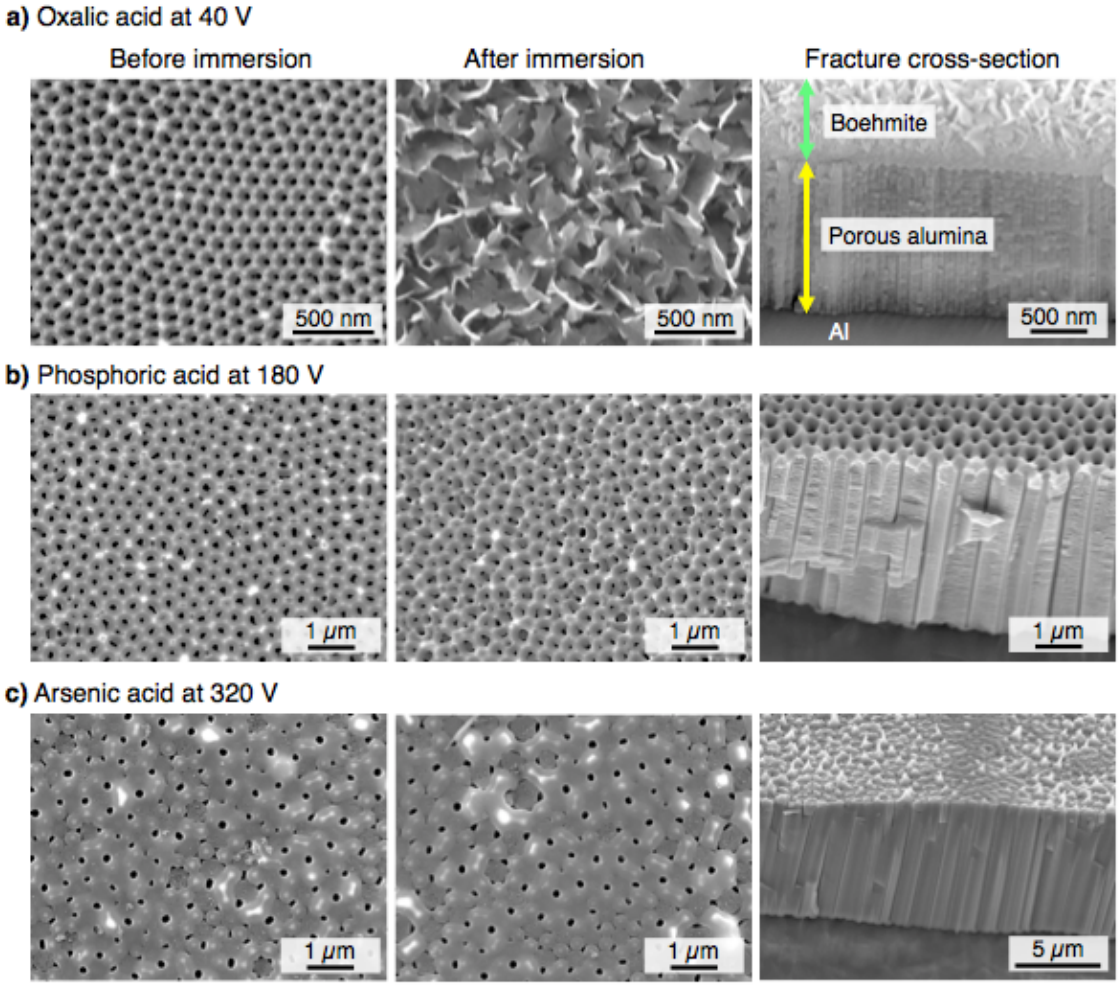
a) Oxalic acid at 40 V
Before immersion
After immersion
Fracture cross-section
Boehmite
Porous alumina
Al
500 nm
500 nm
500 nm
b) Phosphoric acid at 180 V
1 μm
1 μm
1 μm
c) Arsenic acid at 320 V
1 μm
1 μm
5 μm

Figure 8.

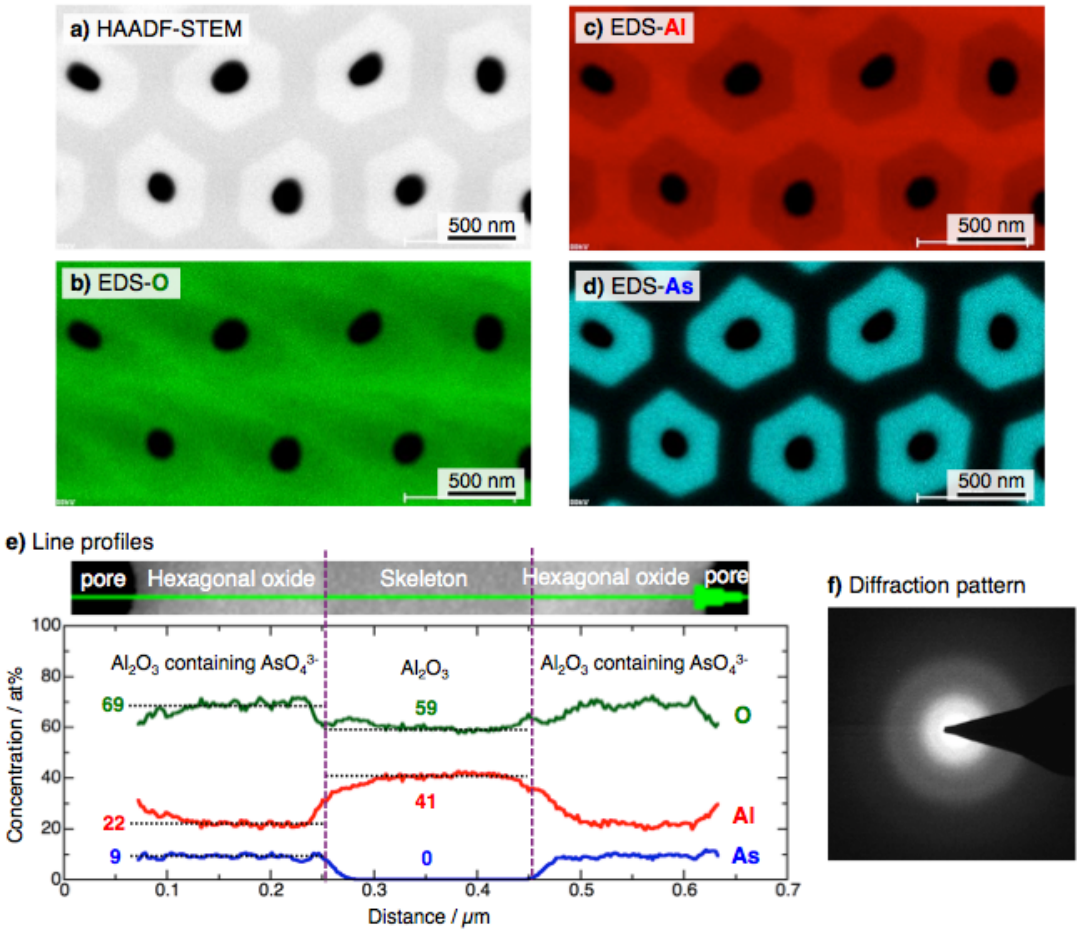
a) HAADF-STEM
500 nm
c) EDS-Al
500 nm
b) EDS-O
500 nm
d) EDS-As
500 nm
e) Line profiles
pore
Hexagonal oxide
Skeleton
Hexagonal oxide
pore
f) Diffraction pattern
Al2O3 containing AsO4 3-
Al2O3
Al2O3 containing AsO4 3-
69
59
O
41
22
Al
9
0
As
Concentration / at%
Distance / μm

Figure 9.

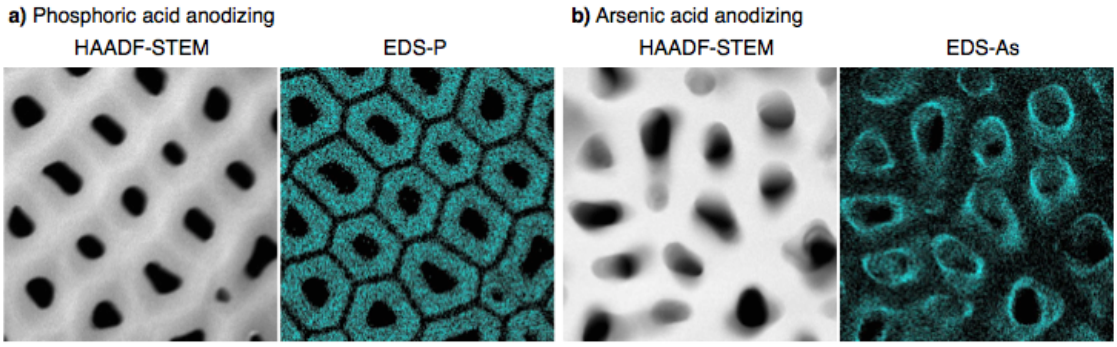
a) Phosphoric acid anodizing
HAADF-STEM
EDS-P
b) Arsenic acid anodizing
HAADF-STEM
EDS-As

Figure 10.

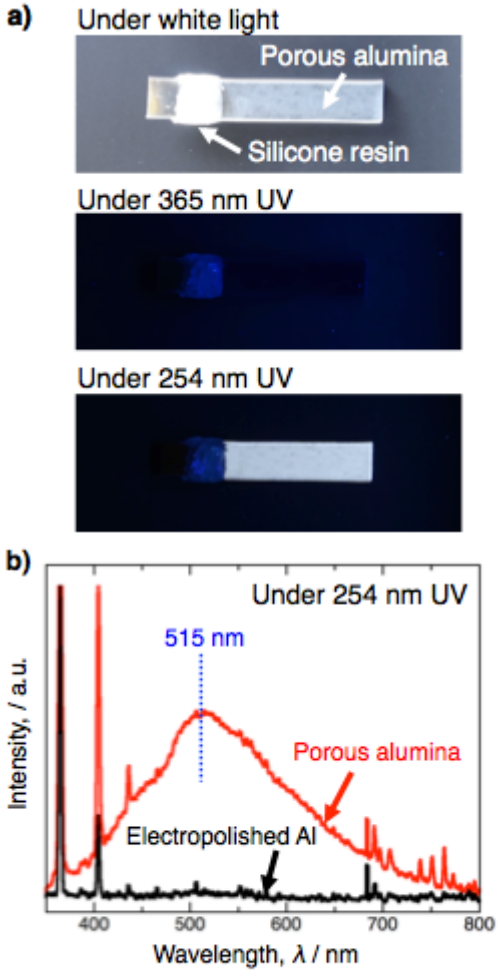
a)
Under white light
Porous alumina
Silicone resin
Under 365 nm UV
Under 254 nm UV
b)
Under 254 nm UV
515 nm
Porous alumina
Electropolished Al
Intensity, / a.u.
400
500
600
700
800
Wavelength, λ / nm

Figure 11.

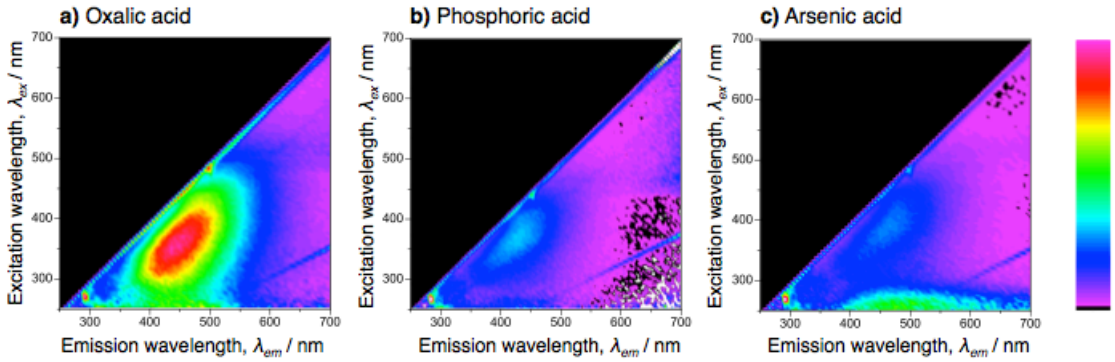
a) Oxalic acid
b) Phosphoric acid
c) Arsenic acid
Excitation wavelength, λ_{ex} / nm
Emission wavelength, λ_{em} / nm
300
400
500
600
700

Figure 12.